TTK4190 Guidance and Control of Vehicles

Assignment 1

M. Brandt & I. Kingman

Problem 1 - Attitude Control of Satellite

Problem 1.1

The satellite dynamics are described by the equation system

$$\begin{aligned} \dot{\mathbf{q}} &= \mathbf{T}_q(\mathbf{q})\boldsymbol{\omega} \\ \mathbf{I}_{CG}\dot{\boldsymbol{\omega}} - \mathbf{S}(\mathbf{I}_{CG}\boldsymbol{\omega})\boldsymbol{\omega} &= \boldsymbol{\tau} \end{aligned} \tag{1}$$

where $\mathbf{I}_{CG} = mr^2\mathbf{I}$ and

$$\boldsymbol{T}\left(\boldsymbol{q}_b^n\right) = \frac{1}{2}\begin{bmatrix} -\varepsilon_1 & -\varepsilon_2 & -\varepsilon_3 \\ \eta & -\varepsilon_3 & \varepsilon_2 \\ \varepsilon_3 & \eta & -\varepsilon_1 \\ -\varepsilon_2 & \varepsilon_1 & \eta \end{bmatrix}. \tag{2}$$

For $\mathbf{q} = [\boldsymbol{\eta}, \boldsymbol{\varepsilon}_1, \boldsymbol{\varepsilon}_2, \boldsymbol{\varepsilon}_3]^\top = [1, 0, 0, 0]^\top$ and $\tau = \mathbf{0}$ we get that

$$\boldsymbol{T}\left(\boldsymbol{q}_b^n\right) = \frac{1}{2}\begin{bmatrix} 0 & 0 & 0 \\ 1 & 0 & 0 \\ 0 & 1 & 0 \\ 0 & 0 & 1 \end{bmatrix}, \tag{3}$$

such that

$$\dot{\mathbf{q}} = \begin{bmatrix} 0 \\ p \\ q \\ r \end{bmatrix} = 0 \quad \Longrightarrow \quad \boldsymbol{\omega} = 0 \tag{4}$$

For $\mathbf{x} = \left[\boldsymbol{\epsilon}^\top, \boldsymbol{\omega}^\top\right]^\top$ the equilibrium point is then simply

$$\mathbf{x}_0 = 0 \tag{5}$$

By multiplying out eq. (1) we get the equations of motion in component form:

$$\dot{\mathbf{x}} = \frac{1}{2}\begin{bmatrix} \eta p - \epsilon_3 q + \epsilon_2 r \\ \epsilon_3 p + \eta q - \epsilon_1 r \\ -\epsilon_2 p + \epsilon_1 q + \eta r \\ 0 \\ 0 \\ 0 \end{bmatrix} + \frac{1}{mr^2}\begin{bmatrix} 0 \\ 0 \\ 0 \\ \tau_1 \\ \tau_2 \\ \tau_3 \end{bmatrix} \tag{6}$$

with the corresponding linearized model

$$\dot{\mathbf{x}} = A\mathbf{x} + B\boldsymbol{\tau}, \tag{7}$$

where

$$A = \left.\frac{\partial \mathbf{f}}{\partial \mathbf{x}}\right|_{\mathbf{x}_0} = \frac{1}{2}\left.\begin{bmatrix} 0 & r & -q & \eta & -\epsilon_3 & \epsilon_2 \\ -r & 0 & p & \epsilon_3 & \eta & -\epsilon_1 \\ q & -p & 0 & -\epsilon_2 & \epsilon_1 & \eta \\ 0 & 0 & 0 & 0 & 0 & 0 \\ 0 & 0 & 0 & 0 & 0 & 0 \\ 0 & 0 & 0 & 0 & 0 & 0 \end{bmatrix}\right|_{\mathbf{x}_0} = \frac{1}{2}\begin{bmatrix} \mathbf{0}_3 & \mathbf{I}_3 \\ \mathbf{0}_3 & \mathbf{0}_3 \end{bmatrix} \tag{8}$$

$$B = \left.\frac{\partial \mathbf{f}}{\partial \boldsymbol{\tau}}\right|_{\mathbf{x}_0} = \frac{1}{mr^2}\begin{bmatrix}\mathbf{0}_3 \\ \mathbf{I}_3\end{bmatrix} \tag{9}$$

Problem 1.2

We will now consider the control law

$$\tau = -\mathbf{K}_d\boldsymbol{\omega} - k_p\boldsymbol{\epsilon} \tag{10}$$

By inserting this control law into the linearized system eq. (7) we find that

$$\dot{\mathbf{x}} = (A - BK)\mathbf{x}, \tag{11}$$

where

$$K = \begin{bmatrix}k_p\boldsymbol{I}_3 & k_d\boldsymbol{I}_3\end{bmatrix} \tag{12}$$

The closed loop transition matrix is then

$$A - BK = \begin{bmatrix}\mathbf{0}_3 & \frac{1}{2}\mathbf{I}_3 \\ -\frac{k_p}{mr^2}\mathbf{I}_3 & -\frac{k_d}{mr^2}\mathbf{I}_3\end{bmatrix} \tag{13}$$

The characteristic polynomial is:

$$\begin{aligned}\Delta(\lambda) &= \det(\lambda\mathbf{I}_3 - (A - BK)) \\ &= \det(\lambda\mathbf{I}_3(\lambda\mathbf{I}_3 + \frac{k_d}{mr^2}\mathbf{I}_3) + \frac{k_p}{2mr^2}) \\ &= \det((\lambda^2 + \frac{k_d}{mr^2}\lambda + \frac{k_p}{2mr^2})\mathbf{I}_3) \\ \Delta(\lambda) &= (\lambda^2 + \frac{k_d}{mr^2}\lambda + \frac{k_p}{2mr^2})^3 = 0\end{aligned} \tag{14}$$

which for $k_p = 2$ and $k_d = 40$ yields

$$\lambda_{1,2} = \lambda_{3,4} = \lambda_{5,6} \approx -0.0278 \pm 0.0248i \tag{15}$$

We observe that the system has thrice repeated complex conjugated poles in the left half plane. The linearized system is therefore stable and the equilibrium point of the nonlinear system is locally asymptotically stable.

In this application one would think poles with a mostly real part is desirable. The open loop linearized system behaves like a marginally stable oscillator (no damping) which makes sense as there is no damping in space. In order to avoid oscillatory behaviour we would want to have a lot of damping in our controller i.e. poles with a mostly real part in the closed loop system.

Problem 1.3

The attitude dynamics of the closed loop system as described in eq. (1) using the control-law given by eq. (10) was simulated using the parameter values as described by table 1. All initial angular velocities were zero. The resulting Euler angles, angular velocity, and control-input are shown in fig. 1, fig. 2, and fig. 3 respectively.

From fig. 1, it is clear that the controller drives the system from the initial angles towards the reference Euler-angles. This response is reflected in the input shown in fig. 3 and the resulting angular velocity shown in fig. 2: As the initial Euler angles are greater (for roll and yaw) or smaller (for pitch) than their target values, the control inputs are equally larger for roll and yaw and negatively larger for pitch in order to accelerate the rotational velocities. As expected, the

Description	Parameter	Value	Unit
Initial pitch	$\phi(0)$	-5	deg
Initial roll	$\theta(0)$	10	deg
Initial yaw	$\psi(0)$	-20	deg
Mass	m	180	kg
Radius	r	2.0	m
Proportional gain	k_p	0.1	–
Derivative gain	k_d	20	–

Table 1: Table of plant parameters used in the simulation of attitude control.

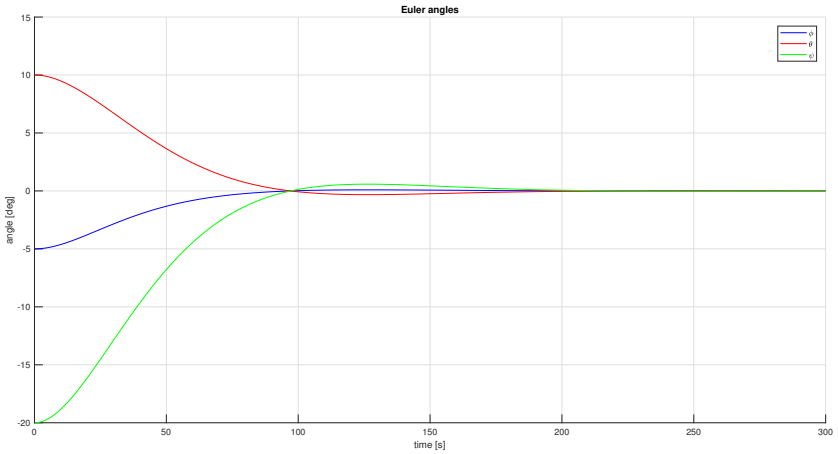

Figure 1: Euler-angles of the satellite using attitude control.

magnitudes of these inputs decrease as the Euler-angles reach their target values. The plant behaves as expected.

In the case of a constant, non-zero reference $\epsilon_{\mathbf{ref}}$, the control-law could be modified by using error coordinates $\tilde{\epsilon}$ in place of the term ϵ in the expression eq. (10) where

$$\tilde{\boldsymbol{\epsilon}} := \boldsymbol{\epsilon} - \boldsymbol{\epsilon}_{ref}. \tag{16}$$

Problem 1.4

We will now consider the modified control law

$$\tau = -\mathbf{K}_d\boldsymbol{\omega} - k_p\tilde{\boldsymbol{\epsilon}} \tag{17}$$

where the quaternion error can be written as

$$\tilde{\mathbf{q}} := \begin{bmatrix} \tilde{\eta} \\ \tilde{\epsilon} \end{bmatrix} = \bar{\mathbf{q}}_d \otimes \mathbf{q} \tag{18}$$

Multiplying out the quaternion product we find $\tilde{\mathbf{q}}$ in component form:

$$\tilde{\mathbf{q}} = \begin{bmatrix} \eta_d \\ -\boldsymbol{\epsilon}_d \end{bmatrix} \otimes \begin{bmatrix} \eta \\ \boldsymbol{\epsilon} \end{bmatrix} = \begin{bmatrix} \eta_d\eta + \boldsymbol{\epsilon}_d^\top\boldsymbol{\epsilon} \\ \eta_d\boldsymbol{\epsilon} - \eta\boldsymbol{\epsilon}_d + S(-\boldsymbol{\epsilon}_d)\boldsymbol{\epsilon} \end{bmatrix}$$

$$\tilde{\mathbf{q}} = \begin{bmatrix} \eta_d\eta + \epsilon_{d1}\epsilon_1 + \epsilon_{d2}\epsilon_2 + \epsilon_{d3}\epsilon_3 \\ \eta_d\epsilon_1 - \eta\epsilon_{d1} + \epsilon_2\epsilon_{d3} - \epsilon_3\epsilon_{d2} \\ \eta_d\epsilon_2 - \eta\epsilon_{d2} + \epsilon_3\epsilon_{d1} - \epsilon_1\epsilon_{d3} \\ \eta_d\epsilon_3 - \eta\epsilon_{d3} + \epsilon_1\epsilon_{d2} - \epsilon_2\epsilon_{d1} \end{bmatrix} \tag{19}$$

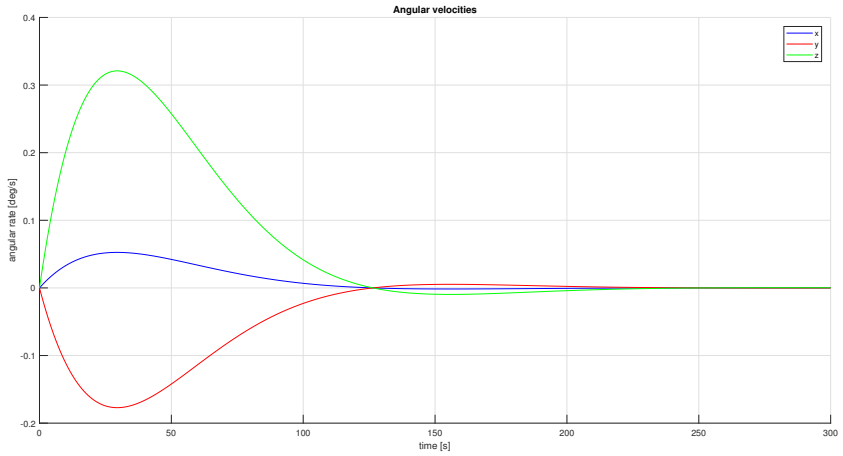

Figure 2: Euler-angle-rates of the satellite using attitude control.

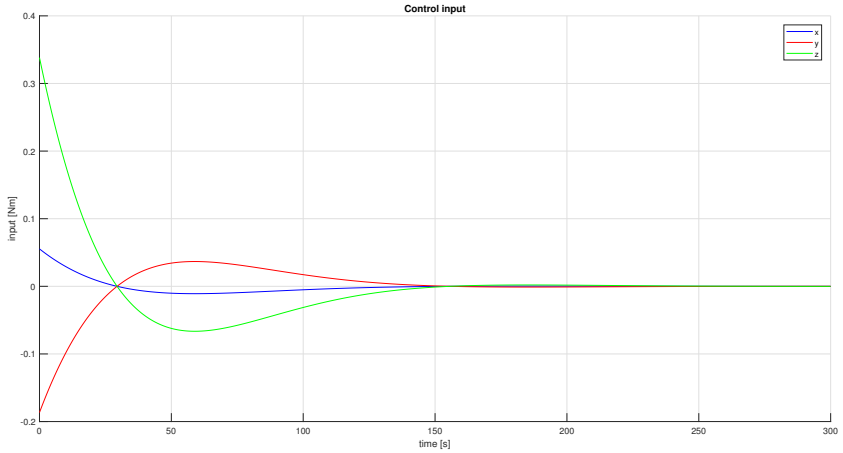

Figure 3: Control input applied to the satellite using attitude control.

Letting $\mathbf{q} = \mathbf{q}_d$ we find that the quaternion error converges at the unit quaternion with $\eta = 1$:

$$\mathbf{q} = \mathbf{q}_d \implies \tilde{\mathbf{q}} = \begin{bmatrix} \eta_d^2 + \epsilon_{d1}^2 + \epsilon_{d2}^2 + \epsilon_{d3}^2 \\ 0 \\ 0 \\ 0 \end{bmatrix} = \begin{bmatrix} 1 \\ 0 \\ 0 \\ 0 \end{bmatrix} \tag{20}$$

Problem 1.5

The attitude dynamics as described in eq. (1) using the modified control-law (17) was simulated using the parameters of table 1, changing the controller gain-parameters such that $k_p = 20$ and $k_d = 400$. The attitude reference was given as a time-varying reference signal $\mathbf{q}_d(t)$ corresponding to $\phi(t) = 0$, $\theta(t) = 15\cos(0.1t)$, and $\psi(t) = 10\sin(0.05t)$.

The resulting Euler angles, angular velocity, control-input, and tracking error are shown in fig. 4, fig. 5, fig. 6, and fig. 7 respectively.

The system behaviour is as expected: With time-varying reference signals for the roll and yaw, the Euler-angles of the system as seen in fig. 4 match their respective input references. Although the

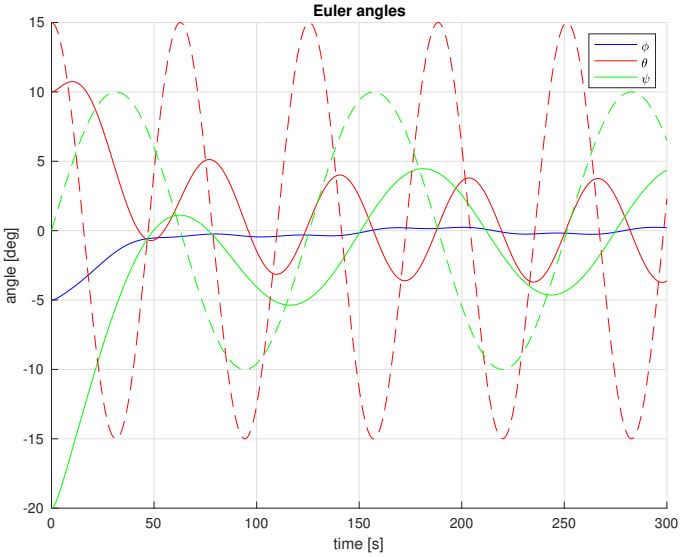

Figure 4: Euler-angles of the satellite using attitude control with a time-varying reference signal.

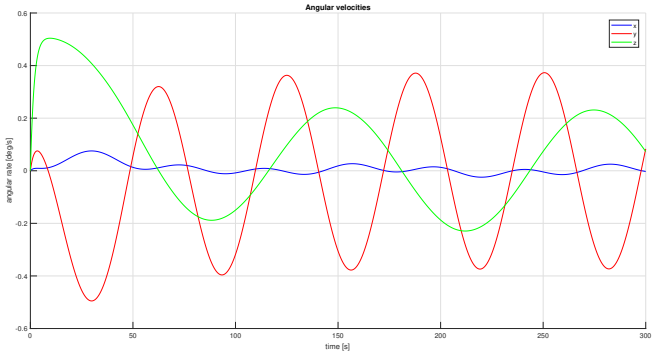

Figure 5: Euler-angle rates of the satellite using attitude control with a time-varying reference signal.

pitch is governed by a zero-reference signal, a slight oscillation can be observed. This is due the fact that the nonlinear attitude dynamics are not completely decoupled.

As with the case with zero reference signal for all angles, a similar transient response is observed initially in order for the system state to go from the initial values of pitch, roll and yaw, to the amplitudes of the sinusoidal reference signals. This is the reason for the very large control input value seen for yaw from $t = 0$ in fig. 6 and the corresponding increase and decrease of yaw rate in fig. 5.

From figure fig. 7, the tracking error for the roll angle is of considerably high amplitude. This is due to the fact that the yaw reference signal amplitude and frequency are both relatively high compared to the systems ability to actuate these signals.The angular velocities have little time to increase or decrease before the sign of the control input has changed. If the frequency of the reference signal were to be increased further, the system would ultimately be driven to a halt for the roll angle.

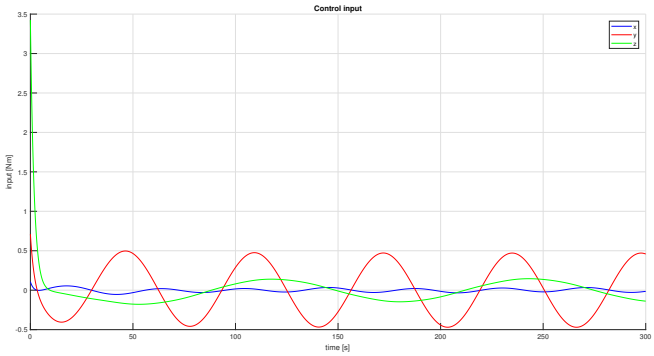

Figure 6: Control input applied to the satellite using attitude control with a time-varying reference signal.

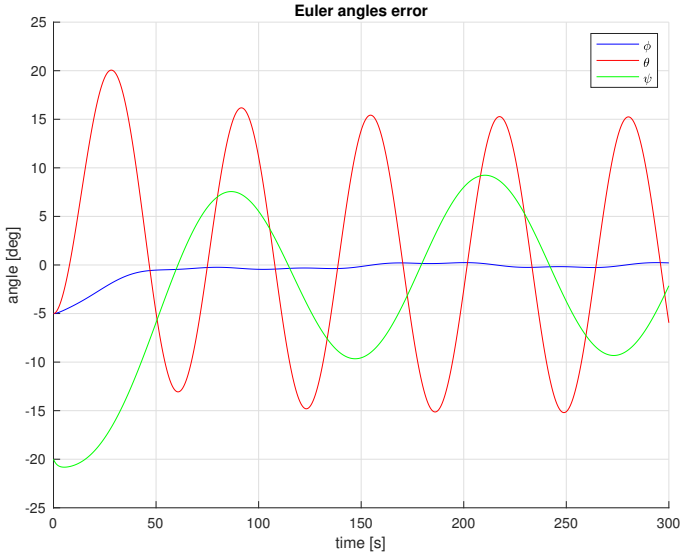

Figure 7: Tracking error of the satellite using attitude control with a time-varying reference signal

Problem 1.6

We will now consider the further modified control law

$$\boldsymbol{\tau} = -\mathbf{K}_d\tilde{\boldsymbol{\omega}} - k_p\tilde{\boldsymbol{\epsilon}} \tag{21}$$

where $\tilde{\omega} = \omega - \omega_{\mathbf{d}}$ is the difference between desired and current angular velocity. It can be shown that the desired angular velocities $\omega_{\mathbf{d}}$ may be calculated from the desired Euler-angles by the equation

$$\boldsymbol{\omega}_d = \mathbf{T}_{\Theta_d}^{-1}(\Theta_d)\dot{\Theta}_d. \tag{22}$$

The dynamics of eq. (1) with the controller given by eq. (21) and eq. (22) were simulated using the same parameters as the above simulation. The resulting angles, angular rates, control inputs, and tracking errors are shown in fig. 8, fig. 9, fig. 10, and fig. 11 respectively.

The system behaves as expected by the same considerations given for the previous simulations. The most noteworthy observation is made by comparing the tracking error with and without desired velocity as part of the control law, that is fig. 11 and fig. 7. The amplitude of the tracking error is

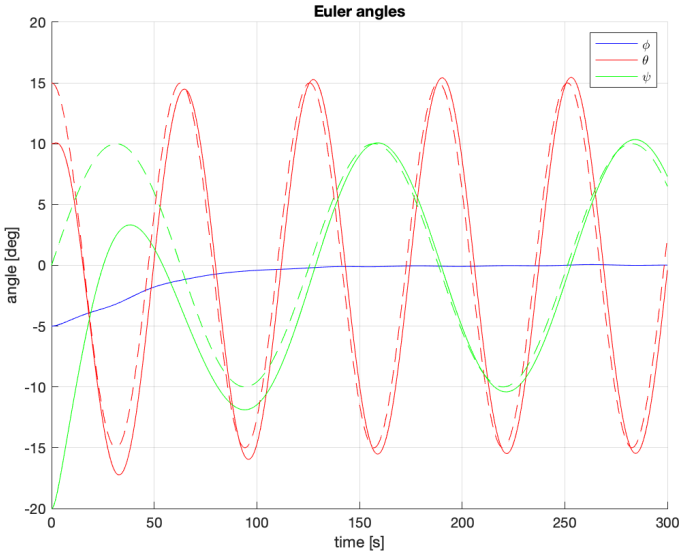

Figure 8: Euler-angles of the satellite using attitude and velocity control with a time-varying reference signal.

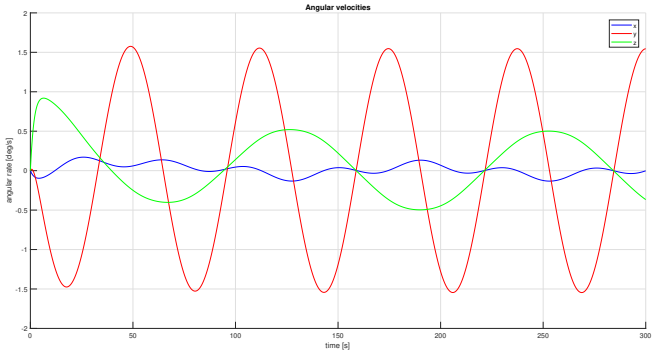

Figure 9: Euler-angle rates of the satellite using attitude and velocity control with a time-varying reference signal.

much smaller when desired angular velocity is used as part of the control law. Consequently, the use of actuation is also considerably higher, as evident by comparing fig. 6 to fig. 10.

The practical significance of this is the trade-off between better control in terms of smaller tracking error using eq. (21) and energy conservation in terms of smaller input amplitude using eq. (17). In layman's terms, one would describe the former control law as smarter, but more wasteful.

The control law might be further improved by introducing acceleration control. That is, the desired angular acceleration could be calculated from the desired angular velocity and implemented in the control law.

Problem 1.7

We consider the Lyapunov function candidate

$$V = \frac{1}{2}\tilde{\boldsymbol{\omega}}^\top \mathbf{I}_{CG}\tilde{\boldsymbol{\omega}} + 2k_p(1-\tilde{\eta}) \tag{23}$$

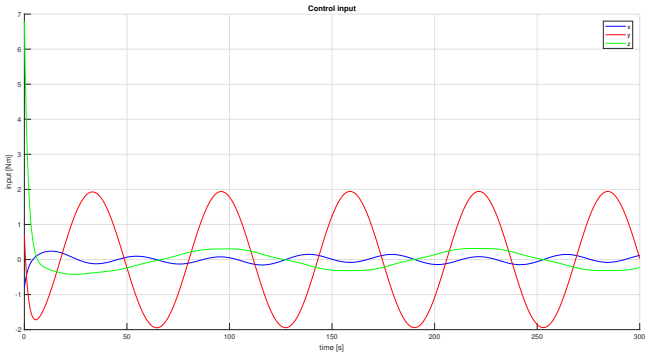

Figure 10: Control input applied to the satellite using attitude and velocity control with a time-varying reference signal.

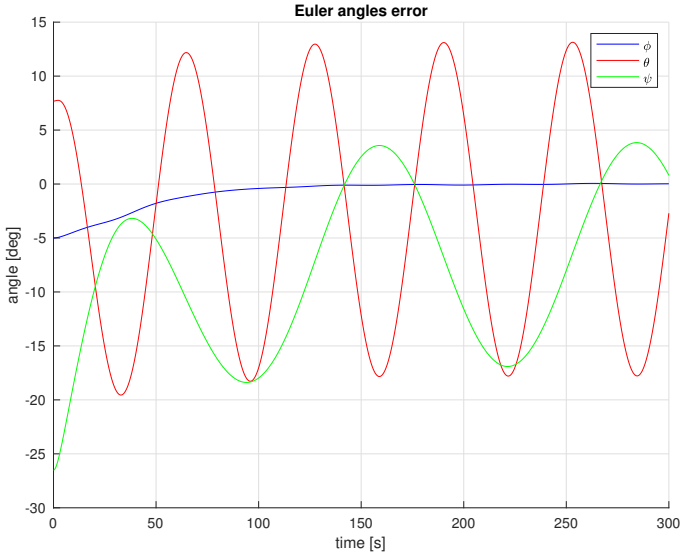

Figure 11: Tracking error of the satellite using attitude and velocity control with a time-varying reference signal.

for setpoint regulation.

Since I_{CG} is positive definite the first term is positive. Since $k_p > 0$ and $|\tilde{\eta}| \leq 1$ the second term is also positive. Therefore the Lyapunov function V is positive. Furthermore since the first term is a quadratic form of $\tilde{\boldsymbol{\omega}}$ we have that $\tilde{\boldsymbol{\omega}} \to \infty \implies V \to \infty$ and V is then radially unbounded.

$$\dot{V} = \tilde{\boldsymbol{\omega}}^\top \mathbf{I}_{CG} \dot{\tilde{\boldsymbol{\omega}}} - 2k_p \dot{\tilde{\eta}} \tag{24}$$

Using the property

$$\dot{\tilde{\eta}} = -\frac{1}{2} \tilde{\boldsymbol{\epsilon}}^\top \tilde{\boldsymbol{\omega}} \tag{25}$$

we get that

$$\dot{V} = \tilde{\boldsymbol{\omega}}^\top \mathbf{I}_{CG} \dot{\tilde{\boldsymbol{\omega}}} + k_p \tilde{\boldsymbol{\epsilon}}^\top \tilde{\boldsymbol{\omega}} \tag{26}$$

Since we are considering setpoint regulation with $\tilde{\boldsymbol{\omega}} = \boldsymbol{\omega}$ we have that

$$\dot{V} = \boldsymbol{\omega}^\top \mathbf{I}_{CG} \boldsymbol{\omega} + k_p \tilde{\boldsymbol{\epsilon}}^\top \boldsymbol{\omega} \tag{27}$$

Then we can manipulate the dynamics such that

$$\mathbf{I}_{CG}\dot{\tilde{\boldsymbol{\omega}}} = \mathbf{I}_{CG}\dot{\boldsymbol{\omega}} = S(\mathbf{I}_{CG}\boldsymbol{\omega})\boldsymbol{\omega} + \boldsymbol{\tau} = S(\mathbf{I}_{CG}\boldsymbol{\omega})\boldsymbol{\omega} - k_d\tilde{\boldsymbol{\omega}} - k_p\tilde{\boldsymbol{\epsilon}} \tag{28}$$

Insert this into eq. (27) we find that

$$\dot{V} = \boldsymbol{\omega}^\top S(\mathbf{I}_{CG}\boldsymbol{\omega})\boldsymbol{\omega} - \boldsymbol{\omega}^\top k_d\boldsymbol{\omega} - \tilde{\boldsymbol{\epsilon}}^\top k_p\boldsymbol{\omega} + k_p\tilde{\boldsymbol{\epsilon}}^\top\boldsymbol{\omega} = \boldsymbol{\omega}^\top S(\mathbf{I}_{CG}\boldsymbol{\omega})\boldsymbol{\omega} - \boldsymbol{\omega}^\top k_d\boldsymbol{\omega} \tag{29}$$

Finally, since $S(\mathbf{I}_{CG}\boldsymbol{\omega})$ is a skew-symmetric matrix $\boldsymbol{\omega}^\top S(\mathbf{I}_{CG}\boldsymbol{\omega})\boldsymbol{\omega} = 0$ such that

$$\dot{V} = -k_d\boldsymbol{\omega}^\top\boldsymbol{\omega} < 0 \quad \forall\boldsymbol{\omega} \neq 0 \tag{30}$$

Notice that $\dot{V}$ is only negative semi-definite, since the expression does not depend on $\boldsymbol{\epsilon}$, only $\boldsymbol{\omega}$. The system is therefore locally asymptotically stable, by Lyapunov's direct method.

Problem 2 - Straight-line path following in the horizontal plane

Problem 2.1

In order to find the simplified 3-DOF model in the horizontal plane we start with the complete 6-DOF model:

$$\begin{bmatrix} \dot{p}^n_{nb} \\ \dot{\Theta}_{nb} \end{bmatrix} = \begin{bmatrix} \boldsymbol{R}(\boldsymbol{\Theta}_{nb}) & \boldsymbol{0}_{3\times 3} \\ \boldsymbol{0}_{3\times 3} & \boldsymbol{T}(\boldsymbol{\Theta}_{nb}) \end{bmatrix} \begin{bmatrix} \boldsymbol{v}^b_{nb} \\ \boldsymbol{\omega}^b_{nb} \end{bmatrix} \tag{31}$$

We then assume that the pitch and roll of the ship will be small and neglect the mechanics of pitch, roll and heave of the ship. By inserting $\phi = 0$ and $\theta = 0$ we find that:

$$\boldsymbol{T}(\boldsymbol{\Theta}_{nb}) = \boldsymbol{I}_3, \quad \boldsymbol{R}_{x,\phi} = \boldsymbol{I}_3, \quad \boldsymbol{R}_{y,\theta} = \boldsymbol{I}_3 \tag{32}$$

such that

$$\dot{\boldsymbol{p}}^n_{nb} = \boldsymbol{R}_{z,\psi}\boldsymbol{v}^b_{nb} \tag{33}$$

and letting $\boldsymbol{\nu} = [u, v, r]^\top$ and $\boldsymbol{\eta} = [x^n, y^n, \psi]^\top$ we get the ship model in the horizontal plane:

$$\dot{\boldsymbol{\eta}} = \boldsymbol{R}_{z,\psi}\boldsymbol{\nu} \tag{34}$$

or equivalently:

$$\begin{aligned} \dot{x} &= u\cos(\psi) - v\sin(\psi) \\ \dot{y} &= u\sin(\psi) + v\cos(\psi) \\ \dot{\psi} &= r \end{aligned} \tag{35}$$

By utilising the trigonometric formulae

$$\begin{aligned} \sin(\alpha+\beta) &= \sin(\alpha)\cos(\beta) + \cos(\alpha)\sin(\beta) \\ \cos(\alpha+\beta) &= \cos(\alpha)\cos(\beta) - \sin(\alpha)\sin(\beta), \end{aligned} \tag{36}$$

and

$$\psi = \chi - \beta \tag{37}$$

it was found that

$$\begin{aligned} \dot{x} &= u(\cos\chi\cos\beta + \sin\chi\sin\beta) - v(\sin\chi\cos\beta - \cos\chi\sin\beta) \\ \dot{y} &= u(\sin\chi\cos\beta - \cos\chi\sin\beta) + v(\cos\chi\cos\beta + \sin\chi\sin\beta). \end{aligned} \tag{38}$$

By using the identities

$$U^2 = u^2 + v^2 \tag{39}$$

$$\cos\beta = \frac{u}{U}, \quad \sin\beta = \frac{v}{U} \tag{40}$$

it was shown that eq. (35) is equivalent to

$$\begin{aligned} \dot{x} &= U\cos(\chi) = U\cos(\psi+\beta) \\ \dot{y} &= U\sin(\chi) = U\sin(\psi+\beta) \end{aligned} \tag{41}$$

Problem 2.2

Using the first order approximations around zero

$$\begin{aligned} \sin(\alpha) &\approx \alpha \\ \cos(\alpha) &\approx 1 \end{aligned} \tag{42}$$

and assuming small values for β acting as a disturbance, the system eq. (41) can be approximated as

$$\begin{aligned} \dot{x} &= U\cos(\psi+\beta) \approx U\cos(\psi) \approx U \\ \dot{y} &= U\sin(\psi+\beta) \approx U\sin(\psi) \approx U\psi \end{aligned} \tag{43}$$

resulting in the system

$$\begin{aligned} \dot{x} &= U \\ \dot{y} &= U\psi \end{aligned} \tag{44}$$

In order for y in the eq. (44) to be the cross-track error in the path-following problem, that is y is the shortest distance between the vessel and a straight path to be followed, the path must coincide with the x-axis in the NED-frame, meaning the vessel is heading north. Consequently one may not follow any straight line in any direction using this approximation, only the x-axis.

Problem 2.3

The first order Nomoto model is

$$\begin{aligned} T\dot{r} + r &= K\delta + b \\ \dot{\psi} &= r \end{aligned} \tag{45}$$

In the Laplace domain we get

$$\psi(s) = \frac{K\delta(s) + b(s)}{s(Ts+1)} \tag{46}$$

Assuming the small value approximation in 2.2, as well as a constant speed U, we also have

$$y(s) = \frac{U}{s}\psi(s) \tag{47}$$

Combining these results yields

$$y(s) = \frac{U(K\delta(s)+b(s))}{s^2(Ts+1)} = \frac{UK}{s^2(Ts+1)}\delta(s) + \frac{U}{s^2(Ts+1)}b(s) \tag{48}$$

We observe that this is a double integrator and therefore need the derivative term to stabilize and the integrator term to handle the rudder bias in the actuation.

Problem 2.4

The 3-DOF horizontal vessel path-following problem was simulated using the Nomoto model as described in eq. (45). A PID-controller for rudder angle input δ

$$\delta = -k_p y - k_d\dot{y} - k_i\int y \tag{49}$$

was implemented, with the goal to follow a path going straight north. The speed U was assumed constant, and the sideslip was assumed to be zero so that $\chi = \psi$. The parameter and controller values are shown in table 2. The controller gains were found through trial and error.

The resulting xy-position, heading angle, heading rate of change, and input rudder angle are shown in fig. 12, fig. 13, fig. 14, and fig. 15 respectively.

From fig. 12 it is observed that the vessel drifts approximately a total of 180m east of the target path before the heading is oriented towards the target path, as seen in fig. 13. When observing the rudder angle in fig. 15, however, it is clear that the controller attempts to correct this behaviour from the beginning, although with considerably small rudder angles. This is due to the fact that the controller gain parameters are of small magnitudes, which was necessitated by the inherently unstable nature of the system as evident by eq. (48), combined with the need for integral effect

Description	Parameter	Value	Unit
Initial x-position	$x(0)$	0	m
Initial y-position	$y(0)$	100	m
Initial heading angle	$\psi(0)$	0	rad
Initial heading rate	$r(0)$	0	rad/s
Speed	U	5	m/s
Bias	b	0.001	rad/s
Nomoto gain	k	0.1	–
Nomoto time constant	T	20	–
Proportional gain	k_p	5×10^{-5}	–
Integral gain	k_i	5×10^{-8}	–
Derivative gain	k_d	1×10^{-2}	–

Table 2: Table of plant parameters used in the simulation of 1. order Nomoto model.

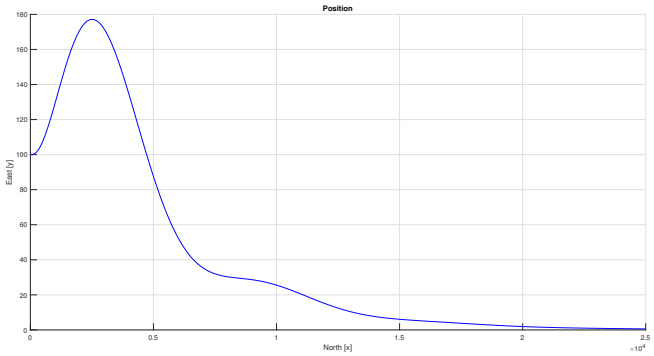

Figure 12: xy-position of the vessel using PID-controller.

due to the rudder bias. Adding integral effect to an already unstable system narrows the space in which the control-gains may be chosen without subjecting the system to a stationary deviation on the one hand, or unstable oscillations on the other.

Next, the same model was simulated using a PD-controller, that is, the control law for the rudder angle was given by

$$\delta = -k_p y - k_d \dot{y}. \tag{50}$$

All other parameter and control gain values remained unchanged. The resulting xy-position, heading, heading rate of change, and control input are shown in fig. 16, fig. 17, fig. 18, and fig. 19 respectively.

The most important result is found by comparing the xy-positions of the vessel using a PID-controller with that of a vessel using a PD-controller, that is fig. 12 and fig. 16. The steady-state of the PD-controlled vessel is clearly subject to a stationary deviation of 200m east of the target path. In fact, the PD-controlled vessel converges to a constant path faster than its PID-counterpart, as evident by comparing the times at which the heading reaches zero in fig. 17 and fig. 13.

This stationary deviation is of course due to the fact that there is a bias in either the rudder or in the form of ocean current. Without the use of integral effect, the controller is not able to "defeat" this bias, resulting in a constant yet insufficient use of non-zero input paired with a constant error between target and true position. This illustrates the challenges and importance of integral action in the control problem.

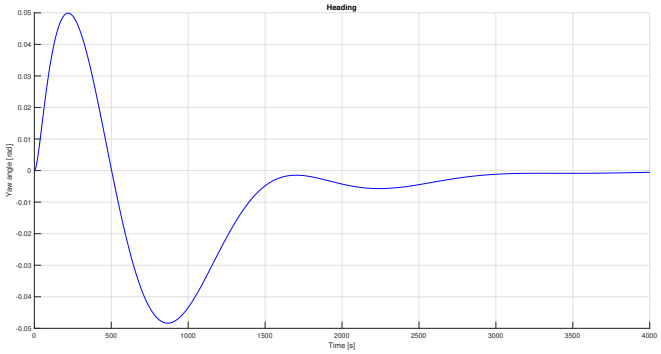

Figure 13: Heading of the vessel using PID-controller.

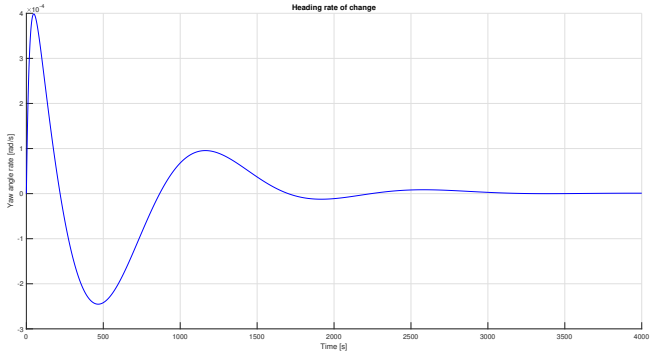

Figure 14: Heading rate of change of the vessel using PID-controller.

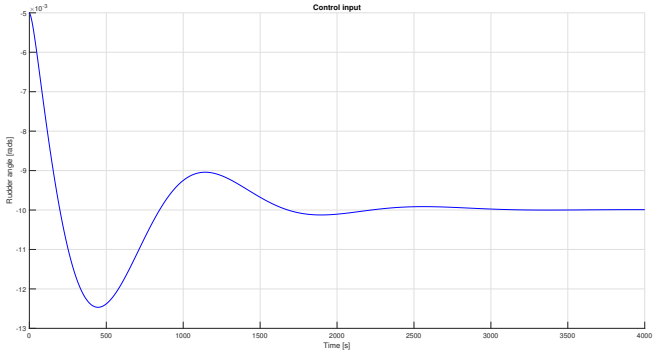

Figure 15: Rudder angle of the vessel using PID-controller.

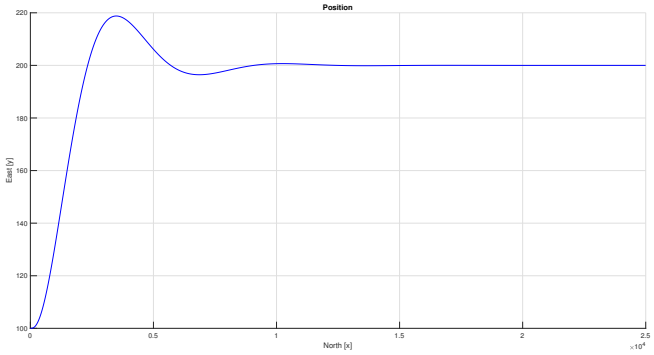

Figure 16: xy-position of the vessel using PD-controller.

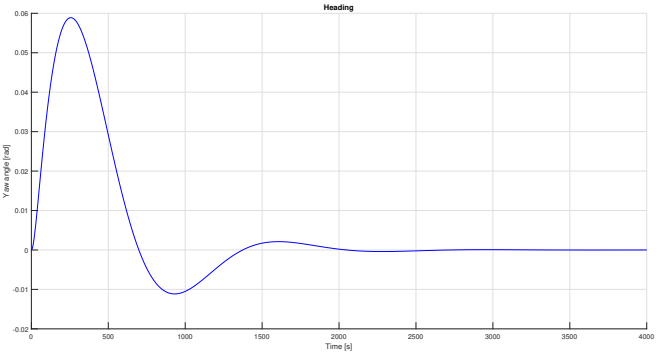

Figure 17: Heading of the vessel using PD-controller.

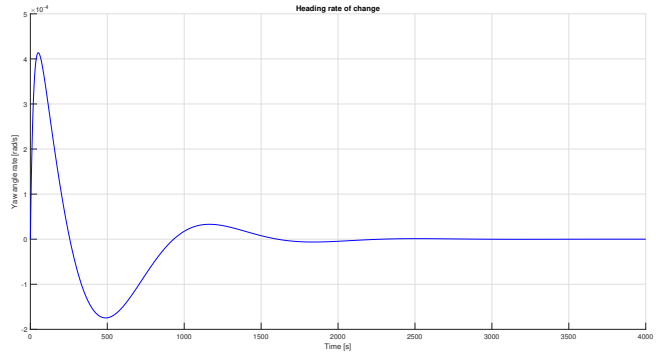

Figure 18: Heading rate of change of the vessel using PD-controller.

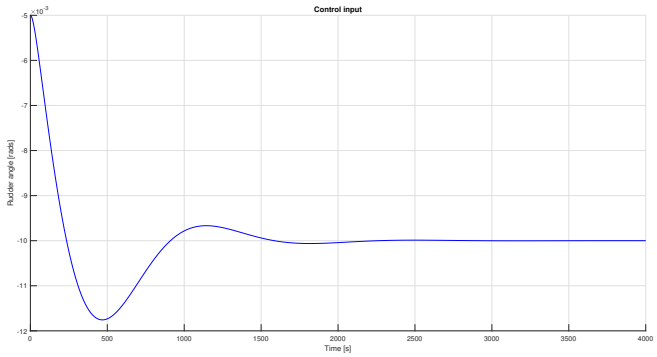

Figure 19: Rudder angle of the vessel using PD-controller.